

Exact Ligand Solid Angles

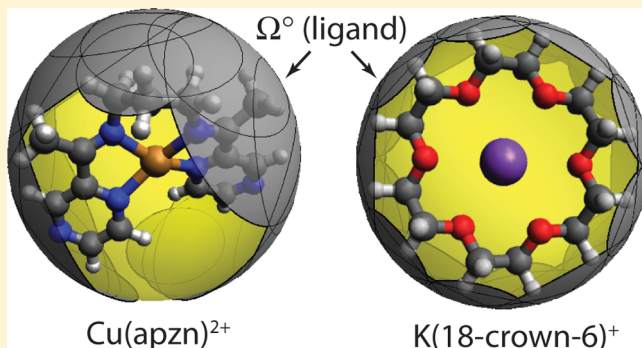
Jenna A. Bilbrey,[†] Arianna H. Kazez,[†] Jason Locklin,[‡] and Wesley D. Allen*,[†]

[†]Department of Chemistry and Center for Computational Chemistry, University of Georgia, Athens, Georgia 30602, United States

[‡]Department of Chemistry and College of Engineering, University of Georgia, Athens, Georgia 30602, United States

Supporting Information

ABSTRACT: Steric demands of a ligand can be quantified by the area occluded by the ligand on the surface of an encompassing sphere centered at the metal atom. When viewed as solid spheres illuminated by the metal center, the ligand atoms generally cast a very complicated collective shadow onto the encompassing sphere, causing mathematical difficulties in computing the subtended solid angle. Herein, an exact, analytic solution to the ligand solid angle integration problem is presented based on a line integral around the multisegmented perimeter of the ligand shadow. The solution, which is valid for any ligand bound to any metal center, provides an excellent method for analyzing geometric structures from quantum chemical computations or X-ray crystallography. Over 275 structures of various metals bound to diverse mono- and multidentate ligands were optimized using B3LYP density functional theory to exhibit exact solid angle (Ω°) computations. Among the intriguing Ω° solutions, Pd(xantphos) and ferrocene exhibit holes in their ligand shadows, and Fe(EDTA)²⁻ has a surprisingly simple shadow defined by only four arcs, despite having a multitude of overlaps among individual shadow cones.



INTRODUCTION

Steric properties of multidentate ligands influence activity and selectivity of organometallic catalysts^{1–4} and affect binding affinities to metal ions through the chelate effect.⁵ The steric demands of a ligand can be gauged by properties of the backbone such as metal (M)–donor (D) bite angles ($\angle D-M-D$) or by the entire ligand encumbrance, as in the cone and solid angle descriptions.^{6,7} Both types of descriptors have shown correlations to catalyst selectivity for a variety of organometallic reactions.^{8–11}

The bite angle of bidentate ligands depends on the donor–donor distance, which is affected by the covalent radius of the chelated metal.¹² Because this radius varies greatly among transition metals,¹³ ascribing a single bite angle to a given ligand is unsatisfactory. However, ligand bite angles can be standardized for chelation to a group of metals with similar radii.¹² The bite angle cannot describe additional steric demands of backbone substituents, the dynamic nature of flexible ligands, or the ability of ligands to mesh into one another.¹⁴

The Tolman cone angle (θ) was developed to measure the steric demands of a monodentate ligand and later extended to bidentate ligands.^{6,15} Experimental “cone angle equivalents” have been assigned by measuring the rates for association of P-donor ligands to metal carbonyls.¹⁶ In a recent publication, we developed an analytic method to determine an exact cone angle (θ°) of any ligand in any environment without approximations such as fixing the M–D bond length, centering the cone on the M–D bond, or averaging apex angles for asymmetrical ligands.¹⁷ Our mathematically rigorous method determines θ°

by exactly solving for the most acute cone possible that contains the entire ligand. Nonetheless, the θ and θ° cone angle approaches are most effective for flexible, monodentate ligands that undergo unhindered rotation and do not satisfactorily treat cases of ligand meshing.¹⁸

An alternative steric descriptor to the Tolman cone angle is the solid cone angle (Θ),^{7,19–21} which is especially beneficial when the ligand is highly asymmetric or rotationally hindered, as in multidentate ligands. Because Θ accounts for indentations in the ligand profile, these parameters should be systematically smaller than their Tolman counterparts, although there is a nonlinear relationship between cone and solid angles.²² In rotationally hindered environments, indentations can allow ligands to mesh together into a more compact shape. The Θ parameter is defined as $2 \cos^{-1}(1 - \Omega / 2\pi)$, where Ω is the solid angle of the complete shadow cast by a ligand when hypothetically illuminated from the metal center. Considered a solid sphere, each ligand atom produces a shadow cone, resulting in a very complicated collective ligand shadow. An arbitrary number of overlapping shadow cones causes daunting analytic difficulties in the computation of Ω . The collective shadow and numerous overlapping cones of the large ligand 2,2'-bis(diphenylphosphino)-1,1'-binaphthyl (BINAP) are depicted in Figure 1.

Because no analytic solution to the solid angle integration problem was known, detailed algorithms were devised in the

Received: May 23, 2013

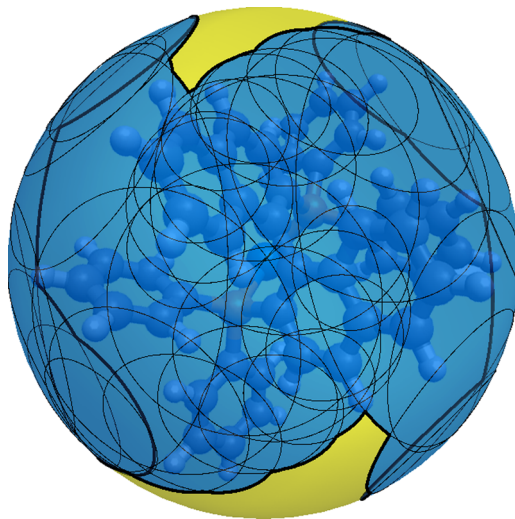


Figure 1. The occluded area (blue) determining the ligand solid angle of Pd(BINAP) results from the intricate overlap of many shadow cones (circles) of the individual atoms. Two indentations (yellow) in the ligand profile are prominent.

1990s to reduce errors in Ω from overlapping shadows. The refined scheme of Taverner et al.^{20,23} is based on the equation

$$\Omega = \sum_i 2\pi(1 - \cos \alpha_i) - \sum_{i>j} A_{ij} + \sum_{i>j>k} A_{ijk} - \sum_{i>j>k>l} A_{ijkl} + \dots \quad (1)$$

in which the leading term is a sum over the solid angles of the individual ligand shadow cones with apex angle α_i , and the successive corrections (A_{ij} , A_{ijk} , A_{ijkl} , ...) approximate the solid angles (Ω_{ij} , Ω_{ijk} , Ω_{ijkl} , ...) of (double, triple, quadruple, ...) overlaps between these cones. In evaluating each (A_{ij} , A_{ijk} , A_{ijkl} , ...) quantity, the ligand shadow is projected from the surface of the encompassing sphere onto an underlying plane (σ_{ij} , σ_{ijk} , σ_{ijkl} , ...) specific to each overlap region. The projection yields intersecting ellipses whose common area is numerically integrated and equated to the corresponding (A_{ij} , A_{ijk} , A_{ijkl} , ...) overlap correction. The procedure is illustrated in Figure 2 for the case of two overlapping shadow cones. The Taverner approach has been supplanted by more direct numerical integration of solid angles in current computer programs such as Solid-G.²²

Assorted other methods to quantify the steric encumbrance of a ligand have been advanced,¹⁹ but none are as widespread as the Tolman and solid angle approaches. Our recent paper on exact cone angles¹⁷ succinctly reviews currently available steric descriptors and some of their applications. Some rely on computed repulsive energies^{24,25} and interaction energies²⁶ between ligand atoms and selectively placed artificial fragments, whereas others are purely geometrical constructs.^{27,28} While many descriptors describe the behavior of individual ligands, few have sought to describe multiple ligand coordination simultaneously.^{22,29–31}

Herein, we present a complete analytic solution to the ligand solid angle integration problem that avoids the surface integral approach and instead uses a line integral around the multisegmented perimeter of the ligand shadow. In this manner, exact ligand solid angles (Ω°) can be evaluated from compact formulas for any ligand of any shape in any

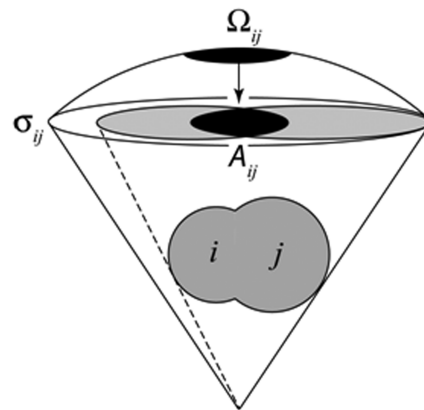


Figure 2. An earlier scheme²³ to account for overlap in ligand solid angle computations. The overlap region (black, above) of the shadow cones of two ligand atoms i and j (gray) on the encompassing sphere subtends a solid angle Ω_{ij} . Projection onto an underlying plane σ_{ij} estimates Ω_{ij} as the overlap area A_{ij} (black, below) common to intersecting ellipses (gray).

environment, with no approximations whatsoever and no need to quantify problematic overlap regions as in eq 1. The designation “exact” in this context refers to the mathematical solution for a given molecular structure, not to the accuracy of the input atomic coordinates. To demonstrate the effectiveness of our method, Ω° and parameters derived from it were computed for over 275 organometallic structures optimized using B3LYP density functional theory with effective core potentials for the transition metals. The applications include a wide array of monodentate phosphine and amine ligands bound to Pd, Ni, and Pt; about 20 multidentate ligands bound to Pd; and miscellaneous multidentate complexes of Cr, Ti, Ni, Cu, Mo, and Fe. Accompanying this report is a computer program to determine the exact solid angle from the Cartesian coordinates of the molecule and any choice of atomic radii, such as traditional Bondi values or more recent alternatives.²²

MATHEMATICAL FORMULATION

The solid angle of an arbitrary closed loop on a sphere can be determined from a line integral around the boundary. To derive an exact formula, the loop is first discretized into an N -sided polygon, and then the limit as N goes to infinity is taken. The solid angle subtended by a geodesic polygon of N sides lying on a unit sphere is given by the known formula:

$$\Omega_N = \sum_j^N \psi_j - (N - 2)\pi \quad (2)$$

where ψ_j denotes the interior angles at the vertices. This equation arises from decomposition of the polygon into geodesic triangles and application of Girard's Theorem.³² Any kinks in the loop where the tangent vectors are discontinuous should be separated from the other vertices before the limit of large N is taken. Thus,

$$\begin{aligned} \Omega_{\text{loop}} &= \lim_{N \rightarrow \infty} \Omega_N \\ &= \sum_j^n \beta_j - (n - 2)\pi - \lim_{N \rightarrow \infty} \sum_j^{N-n} (\pi - \psi_j) \end{aligned} \quad (3)$$

where β_j denotes one of the fixed interior angles of the n kinks.

To compute the vanishingly small $\pi - \psi_j$ angle at a point $\mathbf{u}(t)$ on the curve, consider the adjacent points $\mathbf{v} = \mathbf{u}(t + \Delta t)$ and $\mathbf{w} = \mathbf{u}(t - \Delta t)$. By application of the Spherical Law of Cosines³² to the triangle formed by \mathbf{u} , \mathbf{v} , and \mathbf{w} ,

$$\cos \psi = \csc a \csc b (\cos c - \cos a \cos b) \quad (4)$$

where

$$(\cos a, \cos b, \cos c) = (\mathbf{u} \cdot \mathbf{v}, \mathbf{u} \cdot \mathbf{w}, \mathbf{v} \cdot \mathbf{w}) \quad (5)$$

Using eq 4 to solve for $\sin \psi$, we find

$$\sin \psi = \pm \sqrt{1 - \frac{[\mathbf{v} \cdot \mathbf{w} - (\mathbf{u} \cdot \mathbf{w})(\mathbf{u} \cdot \mathbf{v})]^2}{[1 - (\mathbf{u} \cdot \mathbf{v})^2][1 - (\mathbf{u} \cdot \mathbf{w})^2]}} \quad (6)$$

The quantities in the radicand of eq 6 can be expanded in powers of Δt ; the expansion coefficients are given explicitly in Table S1 of the Supporting Information (SI). Placing these results into eq 6 and invoking the usual expansion $(1 + \delta)^{-1} = 1 - \delta + \delta^2 - \dots$ for small δ , we obtain

$$\begin{aligned} \sin \psi &= \pm \Delta t (\dot{\mathbf{u}} \cdot \ddot{\mathbf{u}})^{-1} \sqrt{(\dot{\mathbf{u}} \cdot \ddot{\mathbf{u}})(\ddot{\mathbf{u}} \cdot \ddot{\mathbf{u}}) - (\dot{\mathbf{u}} \cdot \ddot{\mathbf{u}})^3 - (\dot{\mathbf{u}} \cdot \ddot{\mathbf{u}})^2} \\ &\quad + O[(\Delta t)^2] \end{aligned} \quad (7)$$

Therefore, in the limit of infinitesimal Δt ,

$$d(\pi - \psi) = \pm dt (\dot{\mathbf{u}} \cdot \ddot{\mathbf{u}})^{-1} \sqrt{(\dot{\mathbf{u}} \cdot \ddot{\mathbf{u}})(\ddot{\mathbf{u}} \cdot \ddot{\mathbf{u}}) - (\dot{\mathbf{u}} \cdot \ddot{\mathbf{u}})^3 - (\dot{\mathbf{u}} \cdot \ddot{\mathbf{u}})^2} \quad (8)$$

As N goes to infinity, eq 3 becomes

$$\begin{aligned} \Omega_{\text{loop}} &= \sum_j^n \beta_j - (n-2)\pi - \oint dt p(t) (\dot{\mathbf{u}} \cdot \ddot{\mathbf{u}})^{-1} \\ &\quad \times \sqrt{(\dot{\mathbf{u}} \cdot \ddot{\mathbf{u}})(\ddot{\mathbf{u}} \cdot \ddot{\mathbf{u}}) - (\dot{\mathbf{u}} \cdot \ddot{\mathbf{u}})^3 - (\dot{\mathbf{u}} \cdot \ddot{\mathbf{u}})^2} \end{aligned} \quad (9)$$

where $p(t) = 1$ and $p(t) = -1$ if the curvature vector is directed toward and away from, respectively, the interior of the loop. Assuming that the line integral is performed in a counter-clockwise direction around the loop, we can assign

$$p(t) = \text{sgn}[\mathbf{u} \cdot (\dot{\mathbf{u}} \times \ddot{\mathbf{u}})] \quad (10)$$

The interior angle at the kinks can also be replaced by the (unsigned) turn angle τ_k defined by

$$\beta_k = \pi - p_k \tau_k \quad (11)$$

where $p_k = 1$ and $p_k = -1$ for a turn corresponding to interior angles $<180^\circ$ and $>180^\circ$, respectively. The general equation for the solid angle subtended by an arbitrary loop is thus

$$\begin{aligned} \Omega_{\text{loop}} &= 2\pi - \sum_k^n p_k \tau_k - \oint dt \text{sgn}[\mathbf{u} \cdot (\dot{\mathbf{u}} \times \ddot{\mathbf{u}})] (\dot{\mathbf{u}} \times \ddot{\mathbf{u}})^{-1} \\ &\quad \times \sqrt{(\dot{\mathbf{u}} \cdot \ddot{\mathbf{u}})(\ddot{\mathbf{u}} \cdot \ddot{\mathbf{u}}) - (\dot{\mathbf{u}} \cdot \ddot{\mathbf{u}})^3 - (\dot{\mathbf{u}} \cdot \ddot{\mathbf{u}})^2} \end{aligned} \quad (12)$$

Any curve on the unit sphere can be represented using polar and azimuthal angles (θ, ϕ) that depend on some parameter t . For this purpose, it is convenient to define the orthogonal unit vectors

$$\mathbf{e}_1 = (\sin \theta \cos \phi, \sin \theta \sin \phi, \cos \theta) \quad (13)$$

$$\mathbf{e}_2 = (\cos \theta \cos \phi, \cos \theta \sin \phi, -\sin \theta) \quad (14)$$

and

$$\mathbf{e}_3 = (-\sin \phi, \cos \phi, 0) \quad (15)$$

which obey $\mathbf{e}_1 \times \mathbf{e}_2 = \mathbf{e}_3$, $\mathbf{e}_2 \times \mathbf{e}_3 = \mathbf{e}_1$, and $\mathbf{e}_3 \times \mathbf{e}_1 = \mathbf{e}_2$. The first derivatives of these vectors with respect to the parameter t are

$$\dot{\mathbf{e}}_1 = \mathbf{e}_2 \dot{\theta} + \dot{\phi} \sin \theta \mathbf{e}_3 \quad (16)$$

$$\dot{\mathbf{e}}_2 = -\dot{\theta} \mathbf{e}_1 + \dot{\phi} \cos \theta \mathbf{e}_3 \quad (17)$$

and

$$\dot{\mathbf{e}}_3 = -\dot{\phi} \sin \theta \mathbf{e}_1 - \dot{\phi} \cos \theta \mathbf{e}_2 \quad (18)$$

The vectors required in eq 12 can then be represented as

$$\mathbf{u} = \mathbf{e}_1 \quad (19)$$

$$\dot{\mathbf{u}} = \dot{\theta} \mathbf{e}_2 + \dot{\phi} \sin \theta \mathbf{e}_3 \quad (20)$$

$$\begin{aligned} \ddot{\mathbf{u}} &= -(\dot{\phi}^2 \sin^2 \theta + \dot{\theta}^2) \mathbf{e}_1 + (\ddot{\theta} - \dot{\phi}^2 \sin \theta \cos \theta) \mathbf{e}_2 \\ &\quad + (\ddot{\phi} \sin \theta + 2\dot{\phi}\dot{\theta} \cos \theta) \mathbf{e}_3 \end{aligned} \quad (21)$$

and

$$\begin{aligned} \dot{\mathbf{u}} \times \ddot{\mathbf{u}} &= [\dot{\theta}(\ddot{\phi} \sin \theta + 2\dot{\phi}\dot{\theta} \cos \theta) \\ &\quad - \dot{\phi} \sin \theta(\ddot{\theta} - \dot{\phi}^2 \sin \theta \cos \theta)] \mathbf{e}_1 \\ &\quad - \dot{\phi} \sin \theta(\dot{\phi}^2 \sin^2 \theta + \dot{\theta}^2) \mathbf{e}_2 + \dot{\theta}(\dot{\phi}^2 \sin^2 \theta + \dot{\theta}^2) \mathbf{e}_3 \end{aligned} \quad (22)$$

Therefore,

$$\mathbf{u} \cdot \dot{\mathbf{u}} = g_1(t) = \dot{\theta}^2 + \dot{\phi}^2 \sin^2 \theta \quad (23)$$

$$\begin{aligned} \dot{\mathbf{u}} \cdot \ddot{\mathbf{u}} &= g_2(t) \\ &= \dot{\theta}(\ddot{\theta} - \dot{\phi}^2 \sin \theta \cos \theta) \\ &\quad + \dot{\phi} \sin \theta(\ddot{\phi} \sin \theta + 2\dot{\phi}\dot{\theta} \cos \theta) \end{aligned} \quad (24)$$

$$\begin{aligned} \dot{\mathbf{u}} \cdot \ddot{\mathbf{u}} &= g_3(t) \\ &= (\dot{\phi}^2 \sin^2 \theta + \dot{\theta}^2)^2 + (\ddot{\phi} \sin \theta + 2\dot{\phi}\dot{\theta} \cos \theta)^2 \\ &\quad + (\ddot{\theta} - \dot{\phi}^2 \sin \theta \cos \theta)^2 \end{aligned} \quad (25)$$

and

$$\begin{aligned} p(t) &= \text{sgn}[\dot{\theta}(\ddot{\phi} \sin \theta + 2\dot{\phi}\dot{\theta} \cos \theta) \\ &\quad - \dot{\phi} \sin \theta(\ddot{\theta} - \dot{\phi}^2 \sin \theta \cos \theta)] \end{aligned} \quad (26)$$

The resulting scalar form of eq 12 is

$$\begin{aligned} \Omega_{\text{loop}} &= 2\pi - \sum_k^n p_k \tau_k - \oint dt \\ &\quad \times \frac{p(t)}{g_1(t)} \sqrt{g_1(t)g_3(t) - [g_1(t)]^3 - [g_2(t)]^2} \end{aligned} \quad (27)$$

which is valid for general loops. In applying eq 27, the line integral should be broken up into the intervals between the kinks, as well as regions with the same value of $p(t)$.

As an application of eq 27, consider the solid angle subtended by a partial cone bounded by closed Loop 0 comprising paths A + B + C in Figure 3. Let α_k be the apex angle of the acute cone k , while $\Delta\phi_k$ denotes the change in the local azimuthal angle for the corresponding circular arc on the unit sphere. The vertices (a, b, c) have turn angles $(\tau_a, \tau_b, \tau_c) = (\pi/2, \Delta\phi_1 - \pi, \pi/2)$ and curvature signs $(p_a, p_b, p_c) = (1, -1, 1)$, in order. Table 1 specifies the quantities needed to perform

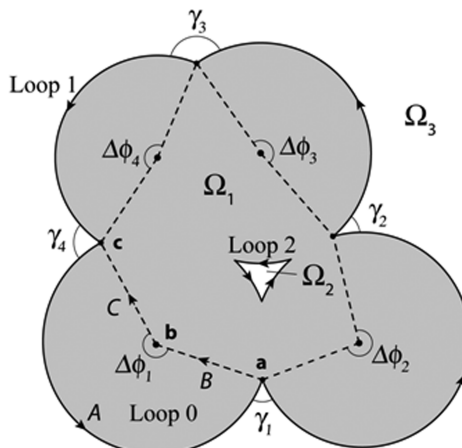


Figure 3. Three possible loops defined by the collective ligand shadow on the surface of the encompassing sphere. Loop 0 comprises paths A + B + C subtending a partial cone; Loop 1 is a convex loop of four arcs and vertices formed by the entire perimeter, and Loop 2 is an interior concave loop with three arcs and vertices bounding a hole in the ligand shadow. The supplement of each turn angle is labeled as $\gamma_k = \pi - \tau_k$.

the line integrals $L = L_A + L_B + L_C$ in eq 27; remarkably, all functions in the integrand are constant, making the integration trivial. Note that the line integrals L_B and L_C are zero, reflecting the fact that arcs along geodesics make no contribution to the solid angle. Inserting the components into eq 27,

$$\begin{aligned}\Omega_{\text{Loop}0} &= 2\pi - \tau_a + \tau_b - \tau_c - L_A - L_B - L_C \\ &= \Delta\phi_1(1 - \cos\alpha)\end{aligned}\quad (28)$$

If $\Delta\phi_1 = 2\pi$, the cone would be complete, and $\Omega_{\text{loop}} = 2\pi(1 - \cos\alpha_1)$, reproducing the standard formula for the solid angle of a cone.

When ligand solid angles are being computed, the arcs on the surface of the unit sphere are formed by intersections with shadow cones; hence, each arc contributes $\Delta\phi_k \cos\alpha_k$ to the line integral, in accord with the exercise above. Figure 3 illustrates the geometric considerations of this application. Two types of loops are encountered, designated here as convex and concave. Traversing the convex perimeter Loop 1 counterclockwise corresponds to positive azimuthal-angle changes $\Delta\phi_k$, and all turn angles have $p_k = -1$ because each interior angle is greater than 180° . In contrast, traversing concave interior Loop 2 counterclockwise involves negative changes in the local azimuthal angles, and all turn angles have $p_k = 1$. However, the solid angle Ω_2 subtended by Loop 2 is already counted in the solid angle Ω_1 computed for Loop 1. Thus, when summing over all loops to obtain the total ligand solid angle (Ω°), the Ω_2 term should be given a negative sign to subtract out the hole in the ligand shadow traced by Loop 2. This type of accounting for all loops leads to an elegant and exact equation for the total ligand solid angle

$$\Omega^\circ = \sum_l^{\text{loops}} \left(2\pi + \sum_k^n \tau_{k,l} - \sum_k^{\text{arcs}} |\Delta\phi_{k,l}| \cos\alpha_{k,l} \right) - 4\pi N_{\text{concave}} \quad (29)$$

where N_{concave} is the number of loops (type 2) whose concave domain is fully contained in the convex domain of some other loop.

To ascertain N_{concave} we recognize that the curvature vector for every arc of each loop points toward the convex domain and that the union of the convex and concave domains for any loop is the entire surface of the unit sphere. In Figure 3, Ω_1 and Ω_2 measure the convex and concave domains of Loop 1 and Loop 2. The region with solid angle $\Omega_3 = 4\pi - \Omega_1$ is in the concave domain of Loop 1 but the convex domain of Loop 2. According to the mathematical definitions of topology, the convex domains discussed here are actually star-convex sets, and the concave domains are technically nonstar-convex sets.

The procedure to determine an exact ligand solid angle via eq 29 is as follows:

(1) From the molecular geometry and an adopted set of atomic radii, determine the axis and apex angle of the shadow cone of each ligand atom.¹⁷

(2) Find all intersection points between the circles on the unit sphere bounding the shadow cones of individual atoms; a list of local azimuthal angles ϕ_{kj} is needed to specify and order the points on cone k where an intersection occurs with cone j .

(3) Identify the boundary arcs that form encompassing loops on the unit sphere; nonboundary arcs can be excluded by showing that their midpoints lie inside the shadow cone of another atom.

(4) Within each boundary loop, compute the $\Delta\phi_k$ local azimuthal angles subtended by each arc on the basis of the ϕ_{kj} list from step 2.

(5) For each vertex point within each loop, compute the turn angle τ_k .

(6) Assemble the components of eq 29 for each loop, and compute the total solid angle Ω° . In practice, no procedure is needed to find N_{concave} , because this quantity must equal the unique integer that places Ω° in the proper interval of $[0, 4\pi]$ steradians.

Attention must now be focused on finding working equations for ϕ_{kj} in step 2 and τ_k in step 5, upon which the solid angle procedure is contingent.

The conditions that determine a point \mathbf{u} on the unit sphere at which the two cones j and k intersect are $\mathbf{u} \cdot \mathbf{n}_j = \cos\alpha_j$, $\mathbf{u} \cdot \mathbf{n}_k = \cos\alpha_k$, and $\mathbf{u} \cdot \mathbf{u} = 1$, where unit vectors \mathbf{n}_j and \mathbf{n}_k specify the cone axes. We can restrict ourselves to apex angles $\alpha_k \leq \pi/2$, because only one branch of the cone equation corresponds to a shadow cast by a ligand atom on the unit sphere. Three coefficients a_{kj} , b_{kj} , and c_{kj} can be used to represent \mathbf{u} as

$$\mathbf{u} = a_{kj}\mathbf{n}_j + b_{kj}\mathbf{n}_k + c_{kj}(\mathbf{n}_j \times \mathbf{n}_k) \quad (30)$$

Applying the three conditions on \mathbf{u} to eq 30 provides

Table 1. Components of the Total Line Integral $L = L_A + L_B + L_C$ of Loop 0

path	$t \in$	$\phi(t)$	$\theta(t)$	$\dot{\phi}$	$\dot{\theta}$	$\ddot{\theta}$	$g_1(t)$	$g_2(t)$	$g_3(t)$	$p(t)$	L_{path}	
A	$(0, \phi_1)$	t	α_1	1	0	0	0	$\sin^2\alpha_1$	0	$\sin^2\alpha_1$	1	$\Delta\phi_1 \cos\alpha_1$
B	$(\pi/2, 0)$	ϕ_1	t	0	0	1	0	1	0	1	0	0
C	$(0, \pi/2)$	0	t	0	0	1	0	1	0	1	0	0

$$\cos \alpha_j = a_{kj} + b_{kj} \cos \alpha_{jk} \quad (31)$$

$$\cos \alpha_k = a_{kj} \cos \alpha_{jk} + b_{kj} \quad (32)$$

and

$$1 = a_{kj}^2 + b_{kj}^2 + 2a_{kj}b_{kj} \cos \alpha_{jk} + c_{kj}^2 \sin^2 \alpha_{jk} \quad (33)$$

with α_{jk} being the angle between the two cone axes,

$$\alpha_{jk} = \cos^{-1}(\mathbf{n}_j \cdot \mathbf{n}_k) \quad (34)$$

Solving eqs 31 and 32 gives the coefficients

$$(a_{kj}, b_{kj}) = (a_{kj}, a_{jk}) = \csc^2 \alpha_{jk} (C_{kj}, C_{jk}) \quad (35)$$

after adopting the definition

$$C_{kj} = \cos \alpha_j - \cos \alpha_k \cos \alpha_{jk} \quad (36)$$

Therefore,

$$\mathbf{u} = \mathbf{w}_{kj} + c_{kj}(\mathbf{n}_j \times \mathbf{n}_k) \quad (37)$$

where

$$\mathbf{w}_{kj} = \csc^2 \alpha_{jk} (C_{kj} \mathbf{n}_j + C_{jk} \mathbf{n}_k) \quad (38)$$

The normalization condition on \mathbf{u} provides

$$c_{kj} = \pm \csc \alpha_{jk} \sqrt{1 - \mathbf{w}_{kj} \cdot \mathbf{w}_{kj}} \quad (39)$$

and after algebraic reduction of the quantity $\mathbf{w}_{kj} \cdot \mathbf{w}_{kj}$, we obtain

$$\mathbf{u} = \csc^2 \alpha_{jk} [C_{kj} \mathbf{n}_j + C_{jk} \mathbf{n}_k \pm D_{jk}(\mathbf{n}_j \times \mathbf{n}_k)] \quad (40)$$

In eq 40

$$\begin{aligned} D_{jk} &= D_{kj} \\ &= \sqrt{1 - \cos^2 \alpha_{jk} - \cos^2 \alpha_j - \cos^2 \alpha_k + 2 \cos \alpha_j \cos \alpha_k \cos \alpha_{jk}} \end{aligned} \quad (41)$$

is the volume of the parallelepiped formed by the vectors \mathbf{n}_j , \mathbf{n}_k and \mathbf{u} . If $|\mathbf{w}_{kj}| > 1$, then no solution exists for \mathbf{u} . If $|\mathbf{w}_{kj}| = 1$, then the arcs just touch on the unit sphere and intersect at a single point \mathbf{w}_{kj} . Otherwise, two intersection points occur.

From the points of intersection, we need to compute the azimuthal angles $\Delta\phi_k$ for each cone, as depicted in Figure 3. For a cone with angle α_k directed along the z axis, the parametric equation for the circle of intersection with the unit sphere is

$$\tilde{\mathbf{u}}(\phi) = (\sin \alpha_k \cos \phi, \sin \alpha_k \sin \phi, \cos \alpha_k) = \mathbf{D}(\alpha_k) \mathbf{q}(\phi) \quad (42)$$

where $\mathbf{q}(\phi) = (\cos \phi, \sin \phi, 1)$ and $\mathbf{D}(\alpha_k)$ is a diagonal matrix with elements $(\sin \alpha_k, \sin \alpha_k, \cos \alpha_k)$. For a general axis \mathbf{n}_k whose polar and azimuthal angles are (θ_k, λ_k) , the coordinates of eq 42 can be rotated using the customary direction cosine matrix Φ .³³ In particular,

$$\mathbf{u}(\phi) = \Phi^T(\theta_k, \lambda_k, 0) \mathbf{D}(\alpha_k) \mathbf{q}(\phi) \quad (43)$$

where the third Euler angle for the rotation has been set to 0 for convenience. The Φ^T matrix in eq 43 has columns composed of the unit vectors in eqs 13–15,

$$\Phi^T(\theta_k, \lambda_k, 0) = [\mathbf{e}_2(\theta_k, \lambda_k) \quad \mathbf{e}_3(\lambda_k) \quad \mathbf{e}_1(\theta_k, \lambda_k)] \quad (44)$$

The reference axis for measuring the local azimuthal angle ϕ lies in the plane formed by the cone axis \mathbf{n}_k and the z axis of the Cartesian coordinate system. By inverting eq 43, we obtain

$$\mathbf{q}(\phi) = \mathbf{D}^{-1}(\alpha_k) \Phi(\theta_k, \lambda_k, 0) \mathbf{u}(\phi) \quad (45)$$

which yields

$$\cos \phi = \csc \alpha_k \mathbf{u} \cdot \mathbf{e}_2(\theta_k, \lambda_k) \quad (46)$$

and

$$\sin \phi = \csc \alpha_k \mathbf{u} \cdot \mathbf{e}_3(\lambda_k) \quad (47)$$

To evaluate the dot products on the right side of eqs 46 and 47 by means of eq 40, first recognize that $\mathbf{n}_j = \mathbf{e}_1(\theta_j, \lambda_j)$ and $\mathbf{n}_k = \mathbf{e}_1(\theta_k, \lambda_k)$, and then determine that

$$\begin{aligned} \mathbf{n}_j \times \mathbf{n}_k &= \sin \theta_j \sin(\lambda_j - \lambda_k) \mathbf{e}_2(\theta_k, \lambda_k) \\ &\quad + [\sin \theta_k \cos \theta_j - \sin \theta_j \cos \theta_k \cos(\lambda_j - \lambda_k)] \\ &\quad \times \mathbf{e}_3(\lambda_k) \end{aligned} \quad (48)$$

With the aid of Table 2, eqs 40, 46, and 47 provide the key results

Table 2. Matrix Elements of $F = \Phi(\theta_j, \lambda_j) \Phi^T(\theta_k, \lambda_k) = \Phi_j \Phi_k^T$

$F_{1j}(\theta_j, \theta_k, \lambda_j - \lambda_k) = \mathbf{e}_1(\theta_j, \lambda_j) \cdot \mathbf{e}_1(\theta_k, \lambda_k)$	$F_{1j}(\theta_j, \theta_k, \lambda_j - \lambda_k) = F_{1j}(\theta_k, \theta_j, \lambda_k - \lambda_j)$
$F_{11} = \sin \theta_j \sin \theta_k \cos(\lambda_j - \lambda_k)$ + $\cos \theta_j \cos \theta_k$	$F_{21} = \sin \theta_k \cos \theta_j \cos(\lambda_j - \lambda_k)$ − $\sin \theta_j \cos \theta_k$
$F_{22} = \sin \theta_j \sin \theta_k$ + $\cos \theta_j \cos \theta_k \cos(\lambda_j - \lambda_k)$	$F_{31} = -\sin \theta_k \sin(\lambda_j - \lambda_k)$
$F_{33} = \cos(\lambda_j - \lambda_k)$	$F_{32} = -\cos \theta_k \sin(\lambda_j - \lambda_k)$

$$\begin{aligned} \sin \phi_{k,j} &= \csc \alpha_k \csc^2 \alpha_{jk} \\ &\quad \times \left\{ C_{kj} \sin \theta_j \sin(\lambda_j - \lambda_k) \right. \\ &\quad \left. \times \left\{ \pm D_{kj} [\sin \theta_k \cos \theta_j - \sin \theta_j \cos \theta_k \cos(\lambda_j - \lambda_k)] \right\} \right\} \end{aligned} \quad (49)$$

and

$$\begin{aligned} \cos \phi_{k,j} &= \csc \alpha_k \csc^2 \alpha_{jk} \\ &\quad \times \left\{ C_{kj} [\sin \theta_j \cos \theta_k \cos(\lambda_j - \lambda_k) - \cos \theta_j \sin \theta_k] \right. \\ &\quad \left. \times \left\{ \pm D_{kj} \sin \theta_j \sin(\lambda_j - \lambda_k) \right\} \right\} \end{aligned} \quad (50)$$

where $\phi_{k,j}$ denotes the local azimuthal angle on cone k for an intersection point with cone j . In general, eqs 49 and 50 must be applied at all intersection points for each cone to determine the azimuthal intervals defining the candidate boundary arcs for the solid angle computation. Among the ligands reported here, the number of arcs for a single cone ranges as high as 34 [d(*t*-Bu)pp and xantphos].

To ascertain the turn angle $\tau_{k,j}$ occurring when an arc on cone k intersects with an arc on cone j , eq 43 can be differentiated to give the required tangent vector formula

$$\mathbf{v}(\phi) = \mathbf{u}'(\phi) = \Phi_k^T \mathbf{D}_k \mathbf{e}_3(\phi) \quad (51)$$

which employs the shorthand notation $\Phi_k = \Phi(\theta_k, \lambda_k)$ and $\mathbf{D}_k = \mathbf{D}(\alpha_k)$. Because $\mathbf{D}_k \Phi_k \Phi_k^T \mathbf{D}_k = \mathbf{D}_k^2$ due to the unitarity of Φ_k , the norm of the tangent vector \mathbf{v}_k for cone k must be $\sin \alpha_k$. The cosine of the turn angle is equal to the dot product of the

normalized tangent vectors for cones k and j . Accordingly, eq 51 yields

$$\cos \tau_{k,j} = \frac{\mathbf{v}_k \cdot \mathbf{v}_j}{|\mathbf{v}_k| |\mathbf{v}_j|} = \csc \alpha_j \csc \alpha_k \mathbf{e}_{3,j}^T \mathbf{D}_j \Phi_j \Phi_k^T \mathbf{D}_k \mathbf{e}_{3,k} \quad (52)$$

Defining the matrix elements $F_{ij}(\theta_j, \theta_k, \lambda_j - \lambda_k)$ as in Table 2, eq 52 simplifies to

$$\cos \tau_{k,j} = (-\sin \phi_{j,k} \cos \phi_{j,k} \ 0) \begin{pmatrix} F_{22} & F_{23} & F_{21} \\ F_{32} & F_{33} & F_{31} \\ F_{12} & F_{13} & F_{11} \end{pmatrix} \begin{pmatrix} -\sin \phi_{k,j} \\ \cos \phi_{k,j} \\ 0 \end{pmatrix} \quad (53)$$

or

$$\begin{aligned} \cos \tau_{k,j} = & F_{33} \cos \phi_{j,k} \cos \phi_{k,j} + F_{22} \sin \phi_{j,k} \sin \phi_{k,j} \\ & - F_{32} \cos \phi_{j,k} \sin \phi_{k,j} - F_{23} \sin \phi_{j,k} \cos \phi_{k,j} \end{aligned} \quad (54)$$

The trigonometric functions of $\phi_{j,k}$ and $\phi_{k,j}$ appearing in eq 54 can be written in shorthand versions of eqs 49 and 50 as

$$\begin{aligned} \sin \phi_{j,k} &= \csc \alpha_j \csc^2 \alpha_{jk} (F_{31} C_{jk} \pm F_{21} D_{jk}) \\ \sin \phi_{k,j} &= \csc \alpha_k \csc^2 \alpha_{jk} (F_{13} C_{kj} \mp F_{12} D_{kj}) \\ \cos \phi_{j,k} &= \csc \alpha_j \csc^2 \alpha_{jk} (F_{21} C_{jk} \mp F_{31} D_{jk}) \\ \cos \phi_{k,j} &= \csc \alpha_k \csc^2 \alpha_{jk} (F_{12} C_{kj} - F_{13} D_{kj}) \end{aligned} \quad (55)$$

Equation 55 reflects the need to switch the choice of signs for the roots when interchanging j, k in order to match intersection points on the two cones.

Placing eq 55 into eq 54, followed by a tedious collection of terms, provides

$$\begin{aligned} & \sin \alpha_j \sin \alpha_k \sin^4 \alpha_{jk} \cos \tau_{k,j} \\ &= C_{jk} C_{kj} [F_{21} (\mathbf{F}^{(1)} \times \mathbf{F}^{(3)})_1 + F_{31} (\mathbf{F}^{(2)} \times \mathbf{F}^{(1)})_1] \\ & \mp C_{jk} D_{kj} [F_{31} (\mathbf{F}^{(2)} \cdot \mathbf{F}^{(1)}) - F_{21} (\mathbf{F}^{(3)} \cdot \mathbf{F}^{(1)})] \\ & \mp D_{jk} D_{kj} [F_{12} (\mathbf{F}_{(3)} \cdot \mathbf{F}_{(1)}) - F_{13} (\mathbf{F}_{(2)} \cdot \mathbf{F}_{(1)})] \\ & - D_{jk} D_{kj} [F_{21} (\mathbf{F}^{(2)} \cdot \mathbf{F}^{(1)}) + F_{31} (\mathbf{F}^{(3)} \cdot \mathbf{F}^{(1)}) \\ & - F_{11} (F_{21}^2 + F_{31}^2)] \end{aligned} \quad (56)$$

In eq 56, $\mathbf{F}^{(j)} = (F_{j1}, F_{j2}, F_{j3})$ and $\mathbf{F}_{(j)} = (F_{1j}, F_{2j}, F_{3j})$ signify the j th row and column of the F_{ij} matrix, respectively, and the subscript 1 outside the parentheses in the first term denotes the first element of the cross product vector. Because the F_{ij} matrix results from a product of unitary matrices Φ_j and Φ_k^T , it also is unitary, having rows and columns that are mutually orthogonal. Therefore, eq 56 simplifies considerably, a manifestation of the independence of each turn angle to collective rotations of the cone axes. Specifically,

$$\begin{aligned} & \sin \alpha_j \sin \alpha_k \sin^4 \alpha_{jk} \cos \tau_{k,j} \\ &= (F_{21}^2 + F_{31}^2) (D_{jk} D_{kj} F_{11} - C_{jk} C_{kj}) \end{aligned} \quad (57)$$

From the definitions in Table 2, $F_{11} = \cos \alpha_{jk}$, and thus $F_{21}^2 + F_{31}^2 = 1 - F_{11}^2 = \sin^2 \alpha_{jk}$, yielding a penultimate equation for the turn angle

$$\cos \tau_{k,j} = \csc \alpha_j \csc \alpha_k \csc^2 \alpha_{jk} (D_{jk} D_{kj} \cos \alpha_{jk} - C_{jk} C_{kj}) \quad (58)$$

Insertion of eqs 36 and 41 into eq 58 with algebraic reduction produces a remarkably simple and completely general formula for the turn angles,

$$\cos \tau_{k,j} = \csc \alpha_j \csc \alpha_k (\cos \alpha_{jk} - \cos \alpha_j \cos \alpha_k) \quad (59)$$

If eq 59 is used to eliminate $\cos \alpha_{jk}$ from eq 41, another useful relationship is found,

$$\sin \tau_{k,j} = \csc \alpha_j \csc \alpha_k D_{kj} \quad (60)$$

In summary, elegant analytic formulas (eqs 49, 50, 59, and 60) have been derived for all quantities required to compute exact solid angles of ligands by means of our line integral formalism (eq 29).

COMPUTATIONAL METHODS

Equilibrium geometric structures for all complexes were optimized using the B3LYP^{34,35} density functional with a radial, angular (75, 302) grid by means of the QChem3.2 package.³⁶ All electronic structure computations employed the Pople basis set 6-31G* for first-row³⁷ and second-row³⁸ atoms and a basis set with the Los Alamos effective core potential, LANL2DZ, for transition metals and halogens.³⁹ Vibrational frequencies were computed at the same level of theory to confirm that all complexes were in fact minima on the potential energy surface. To test geometric variances with respect to theoretical method, a comparison is presented in Table S2 of solid cone angles for a set of 10 monodentate Pd-bound ligands optimized by the B3LYP-D3, M06, B97, M05-2X, and PBE functionals. The mean absolute difference of the Θ° values for these five functionals compared to the B3LYP quantity is 0.6°, 0.9°, 0.3°, 1.4°, and 1.7°, respectively. For two bidentate ligands, dmpe and bpy, the same mean absolute deviation for all five alternative functionals was 1.4° with a standard deviation of 1.9°. These small differences indicate that dependence of the solid angle on the density functional is insignificant in the applications reported here.

A *Mathematica*⁴⁰ package, FindSolidAngle, was written to compute Ω° and Θ° parameters and visualize the solutions, with minimal computational time required for any given input structure. The program is freely available at www.ccqc.uga.edu as of September 1, 2013. Sticking with convention, here we report solid angles derived from the van der Waals atomic radii of Bondi, $r = 1.80, 1.20, 1.70, 1.55, 1.52, 1.47, 1.80, 1.75$, and 2.00 Å for P, H, C, N, O, F, S, Cl, and Fe, respectively.⁴¹ Previous reports have criticized the use of such van der Waals radii to quantify steric demands and have proposed zero energy point radii (r_Z) as alternatives.²² While this issue warrants further study, the focus of this paper is to demonstrate our analytic Ω° method and not to argue for a particular choice of atomic radii or promote a canonical set of steric parameters. With the database of optimized Cartesian structures provided in the SI and ref 17, our FindSolidAngle program can be used to quickly generate results with any set of the atomic radii chosen in future work. To illustrate the dependence of ligand solid angles on the choice of atomic radii, Ω° values derived from Bondi versus r_Z parameters²² are compared for seven selected complexes in Table S3. This table also documents that our analytic procedure applied with r_Z atomic radii yields solid angles in close agreement with the corresponding numerical values we computed with the Solid-G program.²² Scatter plots

Table 3. Computed Exact Solid Cone Angles (Θ°) vs Average Crystallographic Values (Θ°)¹⁹ for Monodentate Ligands

ligand	Θ	$\Theta^\circ(\text{Pd})$		$\Theta^\circ(\text{Ni})$		$\Theta^\circ(\text{Pt})$	
		min	max	min	max	min	max
PM_{e}_3	124	114.3		124.3		119.2	
PEt_3	143	119.0	133.6	128.1	142.0	123.6	136.7
$\text{P}(n\text{-Bu})_3$	148	119.1	134.6	127.9	143.0	123.5	138.2
$\text{P}(i\text{-Bu})_3$	173	<i>a</i>	174.5	<i>a</i>	184.5	<i>a</i>	176.9
$\text{P}(i\text{-Pr})_3$	163	138.7	150.4	146.2	156.7	142.9	154.2
$\text{P}(t\text{-Bu})_3$	182	160.8		168.3		164.7	
$\text{PM}_{\text{e}}_2\text{Et}$	133	115.7	120.7	125.1	129.7	120.4	125.3
$\text{PM}_{\text{e}}_2(i\text{-Pr})$	140	122.9		131.5		127.0	
$\text{PM}_{\text{e}}_2(t\text{-Bu})$	144	129.0		136.9		133.0	
$\text{PM}_{\text{e}}\text{Et}_2$	138	117.3	126.8	126.4	135.5	122.0	130.7
$\text{PEt}_2(i\text{-Pr})$	150	125.5	140.6	134.0	148.8	130.0	144.6
$\text{PEt}_2(t\text{-Bu})$	156	133.2	143.8	141.3	148.9	137.4	145.0
$\text{PM}_{\text{e}}(i\text{-Pr})_2$	151	134.2	137.8	142.8	145.3	134.2	141.6
$\text{PEt}(i\text{-Pr})_2$	156	137.5	145.7	146.5	153.2	141.5	149.9
$\text{P}(i\text{-Pr})_2(t\text{-Bu})$	170	152.0	153.2	160.3	160.3	151.2	157.0
$\text{PM}_{\text{e}}(t\text{-Bu})_2$	163	144.7		152.2		148.8	
$\text{PEt}(t\text{-Bu})_2$	161	147.8	150.5	155.2	157.5	151.7	154.3
$\text{P}(i\text{-Pr})(t\text{-Bu})_2$	178	154.3	156.1	161.8	163.3	158.3	160.1
PPh_3	129	135.7		146.0		140.6	
$\text{P}(p\text{-ClPh})_3$	129	135.8		146.2		140.7	
$\text{P}(m\text{-MePh})_3$	140	135.7	138.8	145.8	148.1	139.7	142.7
$\text{P}(m\text{-ClPh})_3$	136	135.6	137.3	146.2	147.3	140.5	141.7
$\text{P}(p\text{-MePh})_3$	135	135.9		146.0		140.4	
$\text{P}(p\text{-OMePh})_3$	139	135.8	136.1	145.9	146.2	140.2	140.7
$\text{P}(p\text{-FPh})_3$	129	136.0		146.3		140.7	
$\text{P}(m\text{-}(t\text{-Bu})\text{Ph})_3$	159	135.4	154.2	145.3	162.8	140.0	157.7
$\text{P}(o\text{-MePh})_3$	142	141.9	159.9	151.7	169.8	146.4	162.0
PPH_2H	112	125.3		137.3		126.1	
PPH_2Me	124	128.7		139.1		133.4	
PPH_2Et	140	127.4	135.8	135.5	145.4	131.5	140.2
$\text{PPH}_2(n\text{-Bu})$	140	127.3	136.7	135.5	146.0	131.6	140.5
$\text{PPH}_2(i\text{-Bu})$	148	129.3	150.8	137.3	160.8	133.4	154.7
$\text{PPH}_2(i\text{-Pr})$	139	135.4	142.2	143.3	151.2	139.0	146.8
PPH_2Bz	139	129.9	145.8	138.4	155.3	134.6	148.5
$\text{PPH}_2(t\text{-Bu})$	149	141.4		148.6		145.2	
PPH_2Cl	117	129.2		141.1		133.5	
PPhMe_2	126	123.1		132.7		127.9	
PPhEt_2	137	127.7	135.3	136.5	144.0	132.2	139.1
$\text{PPh}(n\text{-Bu})_2$	154	121.9	136.0	130.3	144.2	126.0	140.2
$\text{PPh}(t\text{-Bu})_2$	168	155.2		163.2		159.3	
PBz_3	163	123.0	159.3	131.5	167.7	127.5	158.9
NH_3	87	93.8		112.0		101.9	
NMe_3	124	120.5		131.8		126.4	
NEt_3	142	125.9	148.3	138.6	154.3	132.3	148.0
$\text{N}(i\text{-Pr})_3$	161	152.1	166.1	165.6	176.4	157.7	168.5
NBz_3	173	129.9	156.1	143.2	181.2	137.2	170.6

^aStructure is not a minimum on the potential energy surface. For Cartesian coordinates of all complexes, see ref 17.

comparing results from Bondi versus r_z radii are shown in Figure S1.

More exhaustive checks of our analytic formulas for solid angle integration were executed by means of independent numerical integrations of the surface area of ligand shadows. A 5810-point Lebedev grid was utilized for this purpose.⁴² Each point in the Lebedev grid was tested to ascertain whether it lay inside the shadow of any ligand atom.¹⁷ The fraction of such occluded points multiplied by 4π then gives an estimate of the solid angle of the entire ligand shadow. While inefficient, this Lebedev integration scheme provides a simple, direct check of

the analytic equations. For all complexes investigated in this study, the accuracy of the analytic formulas was confirmed to within the numerical error of the Lebedev integration (≈ 0.01 str), as documented in Table S4.

RESULTS AND DISCUSSION

An extensive collection of data for monodentate phosphine and amine ligands bound to group 10 metals (Ni, Pd, and Pt) is presented in Table 3. Attendant scatter plots appear in Figures S2–S5. Although zero-valent group 10 metals rarely have a single ligand, our complexes were computationally optimized as

Table 4. Steric Parameters of Bidentate Ligands Bound to Platinum^a

ligand	$\angle D-M-D$ (deg)	Θ (deg) ^b	Ω° (str)	Θ° (deg)	G^T (%)
dmpe	100.8	156	5.27	161.4	41.9
depe	100.9	176	5.66	168.6	45.0
d(<i>i</i> -Pr)pe	102.0	188	6.96	192.3	55.4
d(<i>i</i> -Pr)pp	117.6	193	7.42	200.9	59.0
d(<i>t</i> -Bu)pe	103.2	202	7.63	204.7	60.7
d(<i>t</i> -Bu)pp	119.8	210	8.22	215.9	65.4
dcpe	101.7	191	7.03	193.6	55.9
dppm	81.8	168	5.60	167.4	44.6
dppe	100.3	178	6.32	180.7	50.3
dppp	113.3	183	6.85	190.4	54.5
dppb	138.6	188	7.47	201.8	59.4
dppf	133.3	192	7.63	204.8	60.7
BINAP	123.1		7.36	199.7	58.6
BISBI	155.7		8.25	216.4	65.7
xantphos	146.2	192	8.04	212.5	64.0
DIOP	137.4		7.30	198.6	59.1
bpy	80.2		4.09	139.1	32.5

^aCalculated from B3LYP structures using the Bondi atomic radii.^bSolid cone angles compiled from crystal structures of platinum complexes.²¹

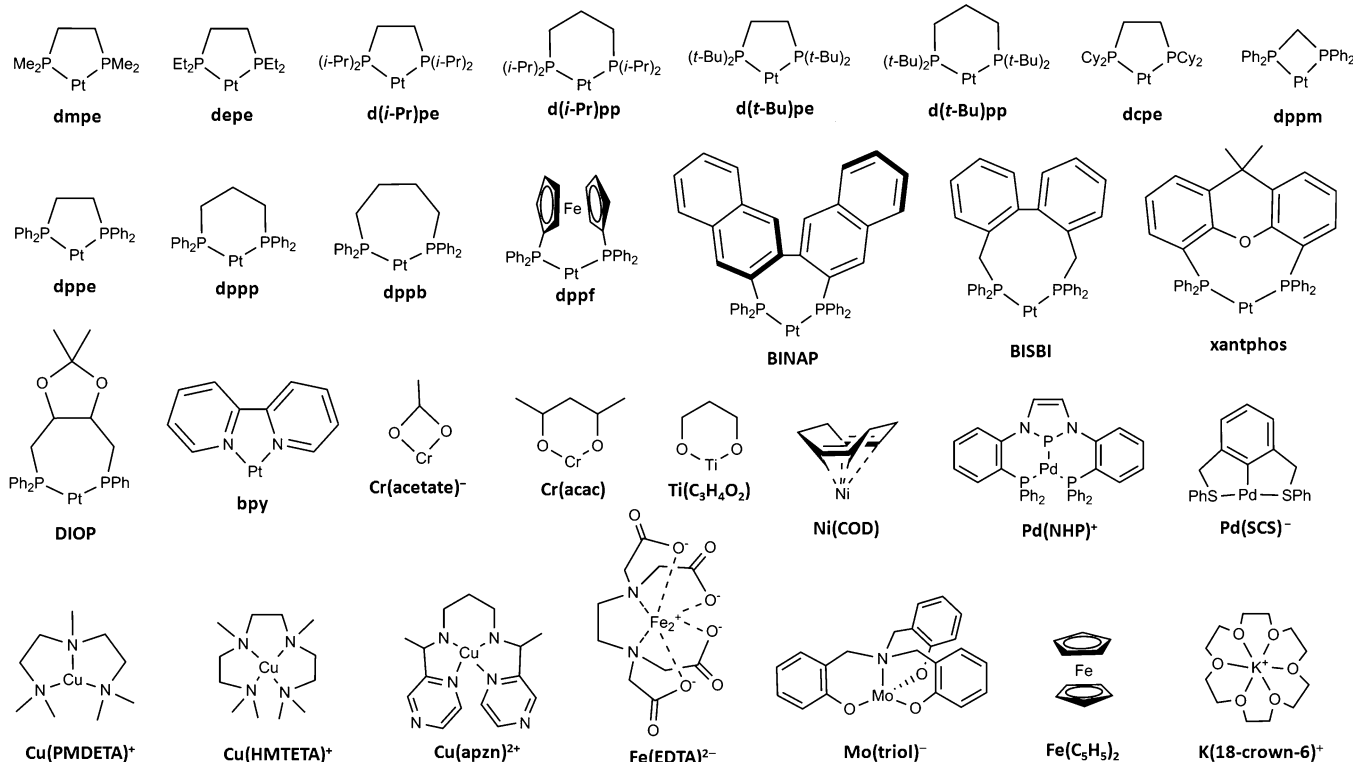
such to provide reference data devoid of steric effects from neighboring ligands. Ligands with multiple conformations exhibit a range of steric values.¹⁷ The minimum (min) and maximum (max) Θ° values for the various conformers are given in separate columns. The Pd(PBz₃) and Ni(PBz₃) cases demonstrate that the min and max Θ° values can differ by 36° or more. In crowded environments, the min conformation is usually more applicable; however, in uncrowded systems the max conformation is preferred, because the corresponding

Table 5. Solid Angles and G-parameters for Multidentate Ligands Corresponding to Chart 1

complex	Ω° (str)	G^T (%)
Cr(acetate) ⁻	4.32	34.4
Cr(acac)	5.61	44.6
Ti(C ₃ H ₄ O ₂)	5.72	45.5
K(18-crown-6) ⁺	7.22	57.5
Ni(COD)	7.53	59.9
Pd(SCS) ⁻	7.82	62.2
Cu(PMDETA) ⁺	8.27	65.8
Cu(apzn) ²⁺	8.45	67.2
Pd(NHP) ⁺	8.78	69.9
Mo(triol) ⁻	9.64	76.7
Cu(HMTETA) ⁺	10.22	81.3
Fe(EDTA) ²⁻	10.34	82.3
Fe(C ₅ H ₅) ₂	12.08	96.1

conformation is of lower energy in almost all cases studied.¹⁷ However, conformations where one arm is min while another is max are certainly possible, but not explored here. The dependence of Θ° on conformation and the possibility of meshing among ligands show that universal values of steric parameters are inadequate and that solid angles should be computed for specific environments.

The steric encumbrance of a given ligand follows the general trend Ni > Pt > Pd as the central metal atom is varied, consistent with the increasing radius of the metal center (the further away the ligand, the less shielding). Solid cone angles do not always increase in proportion to substituent size, as a consequence of overlapping shadow cones. For example, the PdPM₃, PdPEt₃, and PdP(*n*-Bu)₃ complexes exhibit $\Theta^\circ = 114.3^\circ$, 119.0° , and 119.1° , respectively, as the length of the substituent alkyl chain increases.

Chart 1. Structures and Abbreviations of Bidentate Ligands and Multidentate Complexes

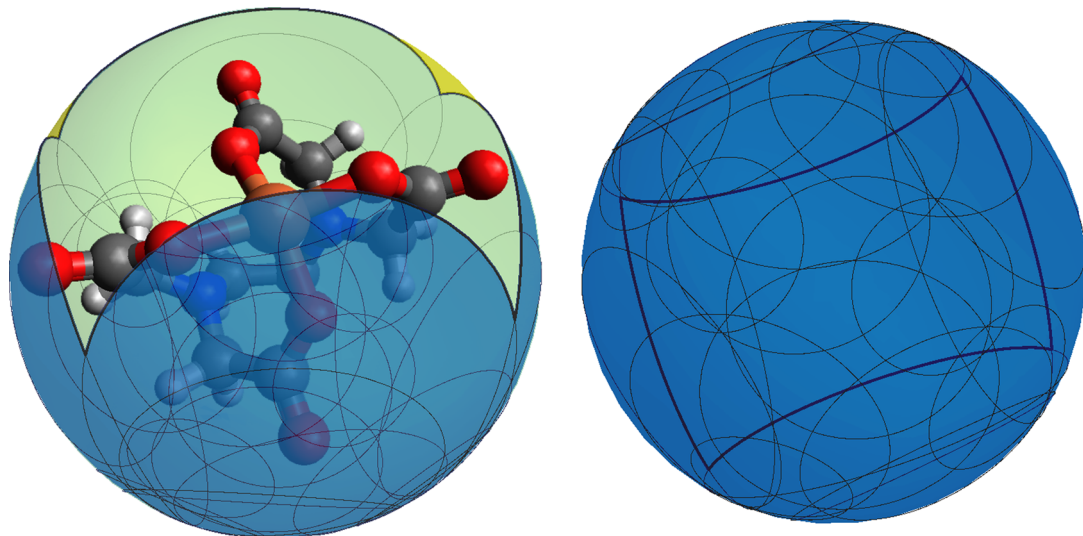


Figure 4. The solid angle (blue) of $\text{Fe}(\text{EDTA})^{2-}$ showing the encapsulated ligand (left) and overlap areas (right). Iron atoms are represented as orange, oxygen as red, nitrogen as blue, carbon as gray, and hydrogen as white.

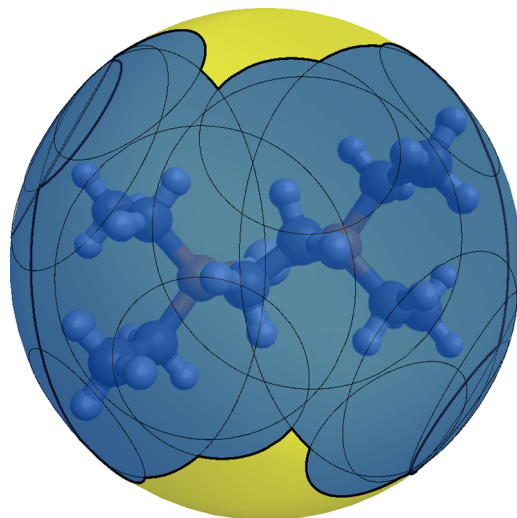


Figure 5. The solid angle (blue) of $\text{Pt}[1,2\text{-bis}(\text{diethylphosphino})\text{-ethane}]$ (depe). Platinum atoms are represented as blue, phosphorus as orange, carbon as gray, and hydrogen as white.

Crowded environments introduce intramolecular interactions between adjacent ligands that frustrate rotation,⁴³ in which case visualization of individual solid angles is helpful in assessing meshing ability. Visualizations of the solid angles for palladium compounds are provided by the depictions in Table S5. Pseudo- C_3 symmetry is generally evident in the indentations of the ligand shadows, though this may change with the addition of adjacent ligands. Two cases showing particularly pronounced indentations and meshing possibilities are the $\text{P}(i\text{-Bu})_3$ and NBz_3 ligands.

Compiled in Table 4 are computed exact solid angles for a variety of platinum-bound bidentate ligands whose structures and abbreviations are shown in Chart 1. These structures are quite rigid, as rotation about either bond is prevented by the increased denticity. In general, the computed Θ° angles are close to the crystallographic values for Pt complexes,²¹ with a MAD of 7.2° and standard deviation of 7.0° (Table S6). By computing the exact solid angle for specific complexes rather than assigning a universal value, a flexible description of steric

properties is achieved that allows for direct study of solid angle dependence on ligand environment.

Guzei and Wendt²² have advocated the use of an easily interpretable G-parameter that describes ligand shielding as a simple percentage of the maximum solid angle of 4π steradians, specifically, $G = 100\Omega/4\pi$. This percentage indicates the remaining open area of a complex where an incoming reagent could bind. Values of G^T computed from our optimized theoretical (T) structures of platinum complexes are also listed in Table 4.

The Ω° parameters in Table 4 show that the commonly used bite angle ($\angle \text{D}-\text{M}-\text{D}$) is not an adequate descriptor of ligand sterics. Although a set of phosphine ligands may have the same backbone, the total steric encumbrance from phosphorus side groups can vary dramatically. For instance, methyl side groups (dmpe) provide $\Omega^\circ = 5.27 \text{ str}$ ($G^T = 41.9\%$), which increases to 6.32 str ($G^T = 50.3\%$) when replaced by phenyl rings (dppe). In stark contrast, dppe has a 0.5° smaller bite angle than dmpe.

Table 5 gives the computed exact solid angles and theoretical G-parameters for a set of multidentate complexes in Chart 1. As an example of how readily our Ω° formulation handles a highly crowded complex, $\text{Fe}(\text{EDTA})^{2-}$ was considered. The EDTA ligand, which has a denticity of six, has $\Omega^\circ = 10.34$, occluding 82.3% of the total unit sphere. The multitude of overlap regions, shown in Figure 4, would be difficult to account for using direct solid-angle integration and subtraction schemes. However, the perimeter of the ligand shadow is defined solely by four carbonyl oxygen atoms, and only four arcs are needed to evaluate the line integral for Ω° . The corresponding azimuthal angle intervals are $\Delta\phi = 98.0^\circ, 154.5^\circ, 98.0^\circ$, and 154.6° , and the vertex turn angles are $\tau = 140.1^\circ, 134.0^\circ, 140.2^\circ$, and 134.0° .

Ligand shadow plots on the unit sphere show gaps in steric coverage that are not accounted for by the Tolman cone angle. For a freely rotating ligand, these gaps may not be relevant, but in a rigid system these gaps can facilitate ligand meshing and should be considered by the steric descriptor. As an example, most of the steric coverage in $\text{Pt}[1,2\text{-bis}(\text{diethylphosphino})\text{-ethane}]$ (depe) comes from the phenyl groups on the phosphorus donors, and not from the ligand backbone. Consequently, there are deep indentations in the shadow of

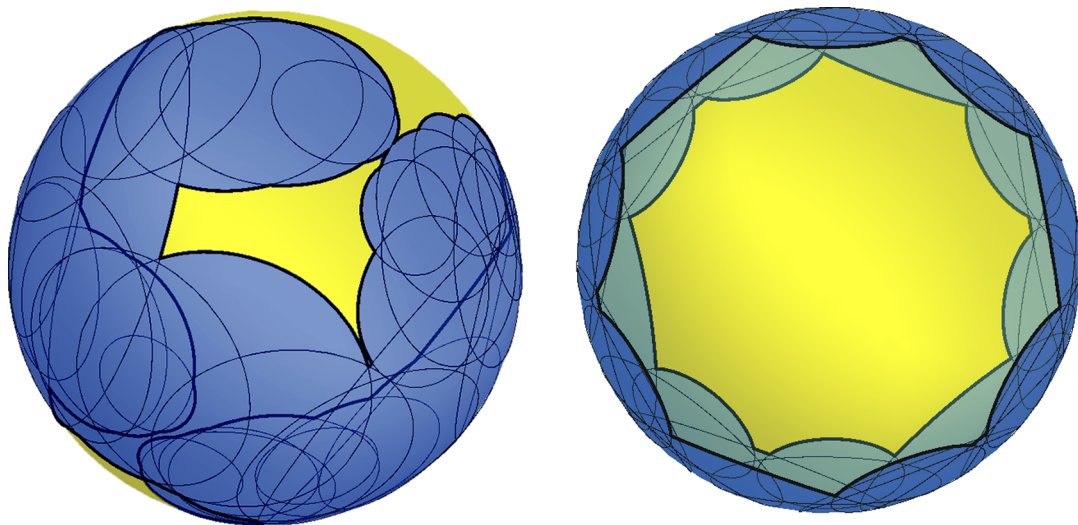


Figure 6. A hole in the solid angle (blue) of $\text{Pd}(\text{xantphos})$ (left) and $\text{K}^+(\text{18-crown-6})$ (right).

the depe ligand (Figure 5), whose overall solid angle is 5.66 str, covering 45.0% of the metal center. Because such gaps may not be chemically relevant if they are small, our *FindSolidAngle* program allows the user to “plug the gap” manually by placing a dummy atom between two arcs that delineate the gap. As an example, plugging one of the gaps in the $\text{Pt}(\text{depe})$ complex gives a solid angle of 6.60 str ($G^T = 52.5\%$), showing that this gap comprises roughly 7.5% of the sphere encompassing the Pd atom.

For the depe ligand, the Tolman bidentate approximation gives a cone angle $\theta = 115^\circ$,⁶ much smaller than either Θ° (168.6°) or θ° (221.8°).¹⁷ The Tolman scheme of surrounding the bidentate ligand with two smaller cones centered around each donor atom is thus strikingly deficient for depe. In many cases, the Tolman semicone angles are determined by physical space-filling models,⁶ which do not reflect distortions from the idealized geometry about the phosphorus atoms. Additionally, ligands with considerably different semicone angles are not well described by the averaging scheme, and the largest substituent spills outside the cone of inclusion.

An interesting situation arises when instead of gaps, there are holes in the ligand shadow, as shown in Figure 6 (left panel) for $\text{Pt}(\text{xantphos})$. Our exact solid angle method handles this situation without difficulty. The outer perimeter of the $\text{Pt}(\text{xantphos})$ profile encloses $\Omega^\circ = 8.06$ str, while the separately reported irregular inner hole comprises $\Omega^\circ = 0.22$ str. Subtracting the latter from the former yields the net solid angle of 7.84 str. However, in this case it is more chemically relevant to include the hole region in the reported solid angle since it is unlikely that any reagent would interact with the metal through such a small area.

Holes can also appear when two separate ligands have overlapping shadows. Ferrocene, a typical metallocene with two η^5 -bound cyclopentadienyl ligands bound to an iron center, displays almost complete enclosure of the metal center with a total G^T value of 96.1%. The boundaries of the shadows of the two cyclopentadienyl rings intersect multiple times, producing five small holes in the overall profile of around 0.1 str each. The meshing of the two ferrocenyl units is handled easily by our mathematical formalism without double-counting the overlap area.

When a large gap is present in the ligand shadow, the hole may have chemical consequences. For complexes of crown ethers such as $\text{K}^+(\text{18-crown-6})$ depicted in Figure 6 (right panel), the ligand forms a belt around the central atom, and two large holes appear in the top and bottom of the solid angle profile, each with exact solid angles of 2.67 str ($G^T = 21.4\%$). Because smaller ligands could potentially access the central potassium atom through either hole, knowing the size of the hole, as well as the size of the incoming ligand, becomes important.

The ligand encumbrance, and thus the solid angle, depends on steric environment.⁴⁴ For example, chromium can have a maximum of three acetylacetone (acac) ligands to give a Ω° of 12.32 str ($G^T = 98.0\%$). Looking at a single acac unit in the $\text{Cr}(\text{acac})_3$ structure gives a Ω° of 4.49 str ($G^T = 35.7\%$) per acac. Thus, in the $\text{Cr}(\text{acac})_3$ structure there is about a 9% overlap of the separate units. To study the amount of ligand compression, we computationally optimized chromium with a single acac unit and found a Ω° of 5.61 str ($G^T = 44.6\%$), which amounts to an 8.9% ligand compression in the full $\text{Cr}(\text{acac})_3$ complex. This case highlights the importance of calculating the solid angle for specific complexes rather than using a universal value for each ligand regardless of the environment.

CONCLUSIONS

An exact, analytic solution to the ligand solid angle integration problem has been derived and implemented for practical computations. The formulation relies on a line integral around the perimeter of the ligand shadow cast on an encompassing sphere, thus eliminating the need for complicated subtraction schemes to avoid overcounting of overlap regions. The exact solid angle (Ω°) method is a general solution for all geometrical arrangements and is applicable to entire complexes as well as individual ligands. A freely available program has been developed to calculate exact solid angles from the Cartesian coordinates of a complex, as given by quantum chemical computations, X-ray crystallography, or any other method.

The exact solid angle method was applied comprehensively by using density functional theory to optimize over 275 structures of organometallic compounds involving diverse mono- and multidentate ligands. As a steric descriptor, Ω° is particularly useful for complexes with frustrated rotation about

metal-donor bonds. The Ω° parameter accounts for gaps in the ligand solid angle profile that can facilitate meshing with adjacent ligands. Such gaps are common in bidentate ligands with alkyl backbones, where donor substituents provide the majority of the steric encumbrance. The Ω° solid angle approach along with our recently advanced exact cone angle θ° formalism¹⁷ provides new tools for understanding and predicting steric effects in organometallic chemistry.

■ ASSOCIATED CONTENT

Supporting Information

Mathematical details, statistical analysis, scatter plots, density functional comparisons, numerical confirmation of Ω° integration formulas, solid angle visualizations, and Cartesian coordinates of complexes. This material is available free of charge via the Internet at <http://pubs.acs.org>.

■ AUTHOR INFORMATION

Corresponding Author

*E-mail: wdallen@uga.edu.

Author Contributions

The application to organometallic compounds and analysis of results was performed by J.A.B. and A.H.K. The mathematical formalism was derived and programmed by W.D.A. The manuscript was written through contributions of all authors. All authors have given approval to the final version of the manuscript.

Funding

This work was supported by the National Science Foundation (CHE 1058631).

Notes

The authors declare no competing financial interest.

■ REFERENCES

- (1) Kranenburg, M.; van der Burgt, Y. E. M.; Kamer, P. C. J.; van Leeuwen, P. W. N. M.; Goubitz, K.; Fraanje, J. *Organometallics* **1995**, *14*, 3081.
- (2) Freixa, Z.; van Leeuwen, P. W. N. M. *Dalton Trans.* **2003**, 1890.
- (3) Breit, B. *Angew. Chem., Int. Ed.* **2005**, *44*, 6816.
- (4) Lanni, E. L.; Locke, J. R.; Gleave, C. M.; McNeil, A. J. *Macromolecules* **2011**, *44*, 5136.
- (5) Schwarzenbach, G. *Helv. Chim. Acta* **1952**, *35*, 2344.
- (6) Tolman, C. A. *Chem. Rev.* **1977**, *77*, 313.
- (7) Immirzi, A.; Musco, A. *Inorg. Chim. Acta* **1977**, *25*, L41.
- (8) Dierkes, P.; van Leeuwen, P. W. N. M. *J. Chem. Soc., Dalton Trans.* **1999**, 1519.
- (9) Culkin, D. A.; Hartwig, J. F. *Organometallics* **2004**, *23*, 3398.
- (10) van Haaren, R. J.; Goubitz, K.; Fraanje, J.; van Strijdonck, G. P. F.; Oevering, H.; Coussens, B.; Reek, J. N. H.; Kamer, P. C. J.; van Leeuwen, P. W. N. M. *Inorg. Chem.* **2001**, *40*, 3363.
- (11) Bessel, C. A.; Margarucci, J. A.; Acquaye, J. H.; Rubino, R. S.; Crandall, J.; Jircitano, A. J.; Takeuchi, K. J. *Inorg. Chem.* **1993**, *32*, 5779.
- (12) Aguilera, D.; Escribano, E.; Speed, S.; Talancon, D.; Yerman, L.; Alvarez, S. *Dalton Trans.* **2009**, 6610.
- (13) Cordero, B.; Gomez, V.; Platero-Prats, A. E.; Reves, M.; Echeverria, J.; Cremades, E.; Barragan, F.; Alvarez, S. *Dalton Trans.* **2008**, 2832.
- (14) Immirzi, A.; Musco, A.; Mann, B. E. *Inorg. Chim. Acta* **1977**, *21*, L37.
- (15) Tolman, C. A.; Seidel, W. C.; Gosser, L. W. *J. Am. Chem. Soc.* **1974**, *96*, 53.
- (16) Hudson, R. H. E.; Poole, A. J. *Organometallics* **1995**, *14*, 3238.
- (17) Bilbrey, J. A.; Kazez, A. H.; Locklin, J.; Allen, W. D. *J. Comput. Chem.* **2013**, *34*, 1189.
- (18) White, D. P.; Anthony, J. C.; Oyefeso, A. O. *J. Org. Chem.* **1999**, *64*, 7707.
- (19) Brown, T. L.; Lee, K. J. *Coord. Chem. Rev.* **1993**, *128*, 89.
- (20) White, D.; Taverner, B. C.; Leach, P. G. L.; Coville, N. J. *J. Comput. Chem.* **1993**, *14*, 1042.
- (21) Niksch, T.; Görts, H.; Weigand, W. *Eur. J. Inorg. Chem.* **2010**, *2010*, 95.
- (22) Guzei, I. A.; Wendt, M. *Dalton Trans.* **2006**, *0*, 3991.
- (23) Taverner, B. C. *J. Comput. Chem.* **1996**, *17*, 1612.
- (24) Caffery, M. L.; Brown, T. L. *Inorg. Chem.* **1991**, *30*, 3907.
- (25) Brown, T. L. *Inorg. Chem.* **1992**, *31*, 1286.
- (26) Fey, N.; Harvey, J. N.; Lloyd-Jones, G. C.; Murray, P.; Orpen, A. G.; Osborne, R.; Purdie, M. *Organometallics* **2008**, *27*, 1372.
- (27) Hillier, A. C.; Sommer, W. J.; Yong, B. S.; Petersen, J. L.; Cavallo, L.; Nolan, S. P. *Organometallics* **2003**, *22*, 4322.
- (28) Clavier, H.; Nolan, S. P. *Chem. Commun.* **2010**, *46*, 841.
- (29) Fischer, R. D.; Li, X.-F. *J. Less-Common Met.* **1985**, *112*, 303.
- (30) Smith, J. M.; Coville, N. J.; Cook, L. M.; Boeyens, J. C. A. *Organometallics* **2000**, *19*, 5273.
- (31) Smith, J. M.; Coville, N. J. *Organometallics* **2001**, *20*, 1210.
- (32) Murray, D. A. *Spherical Trigonometry, for Colleges and Secondary Schools*; Longmans, Green and Co.: London, 1908.
- (33) Zare, R. N. *Angular Momentum: Understanding Spatial Aspects in Chemistry and Physics*; Wiley-Interscience: New York, 1988.
- (34) Lee, C.; Yang, W.; Parr, R. G. *Phys. Rev. B* **1988**, *37*, 785.
- (35) Becke, A. D. *J. Chem. Phys.* **1993**, *98*, 5648.
- (36) Shao, Y.; Fusti-Molnar, L.; Jung, Y.; Kussmann, J.; Ochsenfeld, C.; Brown, S. T.; Gilbert, A. T. B.; Slipchenko, L. V.; Levchenko, S. V.; O'Neill, D. P.; Distasio, R. A., Jr.; Lochan, R. C.; Wang, T.; Beran, G. J. O.; Besley, N. A.; Herbert, J. M.; Yeh Lin, C.; Van Voorhis, T.; Hung Chien, S.; Sodt, A.; Steele, R. P.; Rassolov, V. A.; Maslen, P. E.; Korambath, P. P.; Adamson, R. D.; Austin, B.; Baker, J.; Byrd, E. F. C.; Dachsel, H.; Doerkens, R. J.; Dreuw, A.; Dunietz, B. D.; Dutoi, A. D.; Furlani, T. R.; Gwaltney, S. R.; Heyden, A.; Hirata, S.; Hsu, C.-P.; Kedziora, G.; Khallilin, R. Z.; Klunzinger, P.; Lee, A. M.; Lee, M. S.; Liang, W.; Lotan, I.; Nair, N.; Peters, B.; Proynov, E. I.; Pieniazek, P. A.; Min Rhee, Y.; Ritchie, J.; Rosta, E.; David Sherrill, C.; Simmonett, A. C.; Subotnik, J. E.; Lee Woodcock, H., III; Zhang, W.; Bell, A. T.; Chakraborty, A. K.; Chipman, D. M.; Keil, F. J.; Warshel, A.; Hehre, W. J.; Schaefer, H. F., III; Kong, J.; Krylov, A. I.; Gill, P. M. W.; Head-Gordon, M. *Phys. Chem. Chem. Phys.* **2006**, *8*, 3172.
- (37) Dill, J. D.; Pople, J. A. *J. Chem. Phys.* **1975**, *62*, 2921.
- (38) Francl, M. M.; Pietro, W. J.; Hehre, W. J.; Binkley, J. S.; Gordon, M. S.; DeFrees, D. J.; Pople, J. A. *J. Chem. Phys.* **1982**, *77*, 3654.
- (39) Hay, P. J.; Wadt, W. R. *J. Chem. Phys.* **1985**, *82*, 299.
- (40) *Mathematica*; Wolfram Research, Inc.: Champaign, IL, 2010.
- (41) Bondi, A. *J. Phys. Chem.* **1964**, *68*, 441.
- (42) Lebedev, V.; Laikov, D. *Dokl. Math.* **1999**, *59*, 477.
- (43) Fanizzi, F. P.; Lanfranchi, M.; Natile, G.; Tiripicchio, A. *Inorg. Chem.* **1994**, *33*, 3331.
- (44) White, D.; Coville, N. J. *Adv. Organomet. Chem.* **1994**, *36*, 95.